2-DOF Spherical Parallel Mechanism Capable of Biaxial Swing Motion with Active Arc Sliders

Naoto Saiki [ID], Kenjiro Tadakuma [ID], Masahiro Watanabe [ID], Eri Takane [ID], Masashi Nobutoki,
Shintaro Suzuki, Masashi Konyo [ID], and Satoshi Tadokoro [ID]

Abstract—Most articulated robots comprise multiple joints and links that control the position and posture of the end effector. The kinematic pair arrangement determines characteristics such as output force. The link configurations can be classified as serial link and parallel link mechanisms. A typical parallel link mechanism is the spherical parallel mechanism (SPM), designed to ensure that the end effector has only rotational degrees of freedom. However, the kinematic pair arrangement has not been sufficiently examined in two degrees of freedom (2-DOF) SPMs. Herein, we present a basic design method for the proposed 2-DOF SPM curved biaxial swing mechanism, with inputs comprising arc sliders. The swinging area of the passive link was small, and infinite rotation around a certain axis was achieved without collision or transfer to a singular posture. Using the kinematics of this mechanism, we clarified the linear roll output and non-linear pitch output. Moreover, we fabricated a prototype and measured its basic drive characteristics. The results revealed that the output performance was greatly dependent on the rotation angle, high movable range in the roll axis, and low movable range in the pitch axis.

Index Terms—Mechanism design, actuation and joint mechanisms, parallel robots.

I. INTRODUCTION

MOST articulated robots, such as robotic arms, comprise multiple links and joints that control the position and posture of the end effector. When designing a robot, the kinematic pair arrangement should be initially considered, as it determines

Naoto Saiki is with the Graduation School of Information Sciences, Tohoku University, Miyagi, Sendai 9808579, Japan (e-mail: saiki.naoto@rm.is.tohoku.ac.jp).

Kenjiro Tadakuma is with the Graduation School of Information Sciences and Tough Cyberphysical AI Research Center, Tohoku University, Miyagi, Miyagi Sendai 9808579, Japan (e-mail: tadakuma@rm.is.tohoku.ac.jp).

Masahiro Watanabe is with the Tough Cyberphysical AI Research Center, Tohoku University, Miyagi, Sendai 9808579, Japan (e-mail: watanabe.masahiro@rm.is.tohoku.ac.jp).

Eri Takane is with the Division of Mechanical Engineering, Tohoku University, Aichi, Sendai 9800805, Japan (e-mail: takane@rm.is.tohoku.ac.jp).

Masashi Nobutoki and Shintaro Suzuki are with the Aisin Seiki Corporation, Kariya 4488650, Japan (e-mail: masashi.nobutoki@aisin.co.jp; suzusin@body-t.aisin.co.jp).

Masashi Konyo and Satoshi Tadokoro are with the Graduation School of Information Sciences, Tohoku University, Miyagi Sendai 9808579, Japan (e-mail: konyo@rm.is.tohoku.ac.jp; tadokoro@rm.is.tohoku.ac.jp).

characteristics such as output force, movable range, rigidity, device size, and accuracy. Currently, no mechanism performs perfectly in all aspects because functions and characteristics of each articulated robot change depending on the structure. Therefore, the configuration of links and joints must be designed according to the goal of the robot.

Although there are innumerable articulated robot configurations, the link configurations can be broadly divided into two types: serial and parallel link mechanisms. In general, serial links tend to be configured with fewer links, have a wide workspace (such as work area or range of motions), and their control processes are easy to calculate and implement. Conversely, parallel links have the disadvantage of a small workspace and singular postures with an indefinite mechanical shape; however, the drive torque can be distributed to multiple actuators. Therefore, parallel links have the advantage of reducing the torque required for each actuator. Additionally, owing to the closed-loop structure, errors due to link deformation are averaged without accumulation, thus making the mechanism highly accurate. Furthermore, it is easy to modularize the components and make the structure symmetric, thus simplifying the placement of the center of gravity at the center of the mechanism [1], [2].

One type of parallel link mechanism is the spherical parallel mechanism (SPM). The SPM is designed such that the end effector's rotational degrees of freedom are only around a fixed center. This is suitable for applications that need to change the posture of the end effector while always pointing the control device toward the fixed center.

In this study, we propose a novel two degrees of freedom (2-DOF) SPM, as shown in Fig. 1, called a curved biaxial swing mechanism. This mechanism controls the posture of a Λ-shaped end effector comprised of two arc-shaped shafts that intersect at a constant angle by controlling the positions of two arc sliders. By using sliders instead of general rotary joints as the input, a small swinging motion of the passive link can be maintained. Compared with a conventional 2-DOF SPM, the proposed mechanism can circulate infinitely around a certain axis without collision or transfer to a singular posture.

This study aims to 1) construct a basic design method for 8R slider type 2-DOF SPM capable of infinite rotation in the roll direction without transition to a singular point and 2) measure its basic driving characteristics using a prototype. The achievements of this study help expand and diversify the workspace of 2-DOF SPMs for practical applications in areas not available until now.
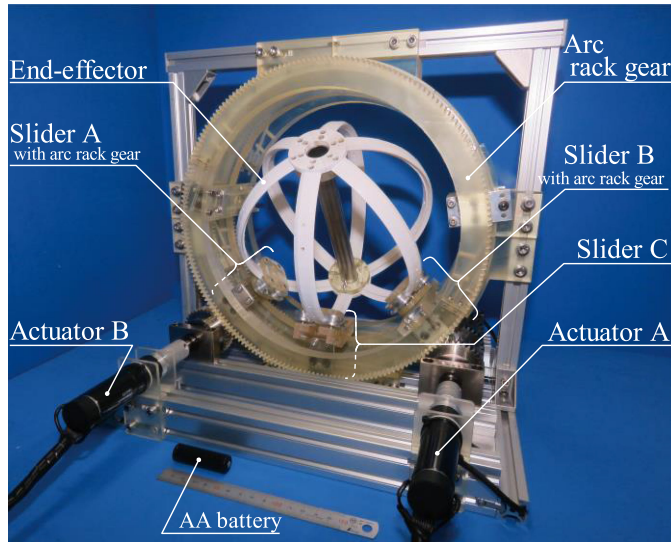
Fig. 1. Overview of the active prototype model of the 2-DOF Spherical Parallel Mechanism.

Fig. 2. Plane type 2-DOF parallel mechanism.

In Section II, we first classify the 2-DOF spherical mechanism and clarify the kinematics and workspace of the devised mechanism to formulate its operation and drive characteristics. Section III describes the concrete mechanical design for embodying the prototype machine. In Section IV, the input-output characteristics and workspace are measured experimentally using a prototype machine, and the results are analyzed. Section V discusses the primary causes of output error observed in experiments and mentions measures to reduce the error. Finally, Section VI concludes the study and presents the scope for future research.

II. Curved Biaxial Swing Mechanism

A. Classification of 2-DOF Spherical Mechanism

Table I shows the classification of 2-DOF spherical mechanisms and their characteristics. Through this paper, R and R denote passive revolute pairs and actuated revolute pairs, respectively. (a) and (b) are 2-DOF spherical serial mechanisms (2-DOF SSMs), which can be composed of a combination of rotating joints or sliders. The primary characteristics of 2-DOF SSMs are infinite rotation and structure simplicity in principle [3]. Conversely, (c), (d), (e), and (f) are 2-DOF SPMs [4]–[6].

The first 2-DOF SPM was designed by Gosselin and Caron in 1999 [4]. Since then, various 2-DOF SPMs have been studied and are expected to be implemented in many fields, such as wrists or hip joints of humanoid robots, pointing devices for cameras, antennas, or telescopes, surgical robots, and stabilization platforms [5]–[16].

2-DOF SPMs can be classified into four types according to the number of revolute pairs and the presence or absence of a slider. Within the four types, 5R SPM with five revolute pairs (rotating joints or arc sliders) and 8R SPM with eight revolute pairs comprise the two groups. Both groups feature a link type
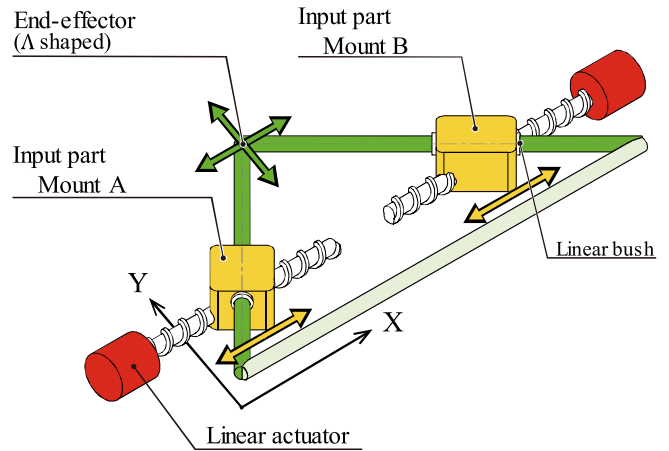
mechanism consisting only of arc links without sliders and a slider type mechanism that includes arc sliders.

The 5R link type SPM listed in Table I(c) can control the end effector's posture by actively driving the two rotating joints with an actuator. About this mechanism, various configurations can be taken, but the theoretical workspace of the mechanism has been studied systematically[17], [18]. In addition, various approaches for kinematic problem and control strategies have been previously studied for this mechanism [12], [13], [19], [20]. The 5R slider type SPM listed in Table I(d) is a mechanism in which two arc-shaped links are manipulated to ensure that the position of the slider on the rims is moved, thus enabling the control of the end effector's posture.

The 8R link type SPM listed in Table I(e) is a mechanism with a base and end effector connected with one RR brunch and two RRR brunches. The forward displacement analysis of the 8R link type SPM is simpler than the 5R link type SPM [6].
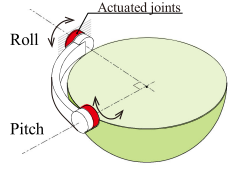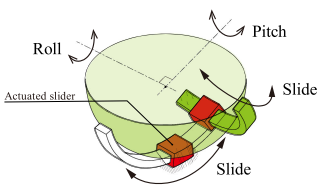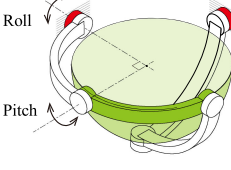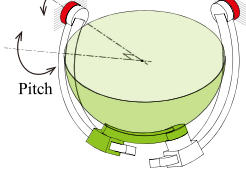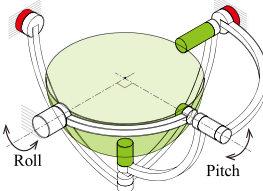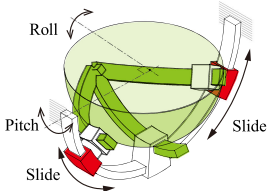
Unlike these conventional configurations, we propose a new 2-DOF SPM (8R slider type SPM), as shown in Table I(f), called a curved biaxial swing mechanism. By controlling two arc sliders, a Λ-shaped end effector swings on the roll and pitch axes. The swing area of the passive links is small compared to SPMs that utilize rotating joint input.

Unlike general parallel link mechanisms, the proposed mechanism can rotate infinitely around a roll axis without any link collision or transfer to a singular posture. Therefore, this mechanism is advantageous for application to wrist joints of robotic arms, actuation parts of machine tools, and 2-DOF centrifugal stirrers that require infinite rotation. However, there is a limit to the movable range of rotation around the pitch axis, as the input-output characteristics change according to the posture. In subsection II. C, we address this issue by analyzing the rotational movement.

B. Principles of 2-DOF Parallel Mechanism with Sliders

In order to realize a planar motion of 2-DOF, a method was proposed in which the two left and right input mounts drive the Λ-shaped end effector as shown in Fig. 2. In this mechanism,

TABLE I
2-DOF SPHERICAL SERIAL AND PARALLEL MECHANISM

Mechanism	Link type	Slider type
2R SSM	(a) Infinite rotation is possible around the roll and pitch, but wiring routing is challenging.	(b) Infinite rotation is possible around the roll and pitch, but wiring routing is challenging [3].
5R SPM (RR-RRR)	(c) Infinite rotation around the roll and pitch is challenging because of collision and singularity [4].	(d) Infinite rotation is impossible because of collision [5].
8R SPM (RR-RRR-RRR)	(e) Infinite rotation is impossible because of collision [6].	(f) Curved biaxial mechanism proposed in this study. Infinite rotation is possible around the roll without transferring to singularity.

the frame shaft of the end effector is connected with the mount via a linear bush. In this configuration, the mounts in the X-axis direction by the linear actuator, but the end effector can perform X–Y translational motions depending on the relative positions of the mounts. While maintaining a relative distance, the end effector moves synchronously with the two mounts along the X-axis. On the other hand, the linear bushes slide when the distance changes between the mounts, and the end effector moves along the Y-axis. The advantage of this mechanism is that the weight of the driven part can be reduced and symmetrical structure can be achieved by deploying actuators coaxially. Leveraging this, we developed a haptic 2-DOF buttock skin stretch device [17] equipped with this driving mechanism.

In this study, we propose a 2-DOF SPM, as shown in Fig. 3. This is a spherical surface of the parallel link mechanism referenced above with 2-DOF in the plane.

While maintaining the mechanical characteristics of the plane type, this mechanism can be regarded as converting a 2-DOF translation output into a 2-DOF rotation around the fixed center of the spherical end effector. Its main components are the left and right input mounts that slide on the arc-shaped base frame and an end effector comprising two arc-shaped frame shafts that intersect at a constant angle α. The arc-shaped base frame and end effector share the same center as the sphere.

With this structure, the end effector rotates around the X-axis (roll axis) when the left and right mounts move while
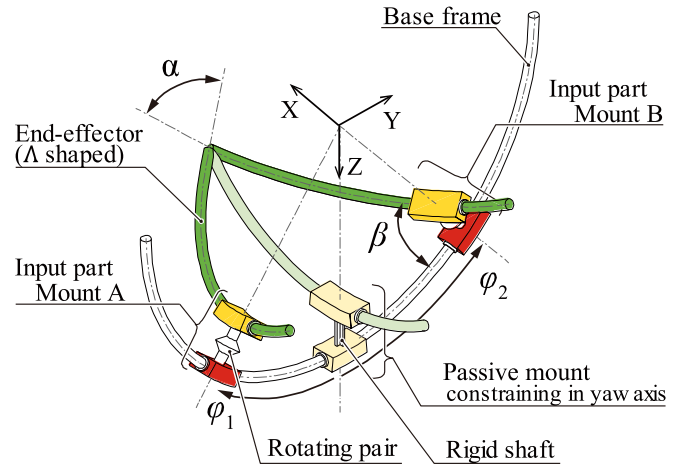
Fig. 3.   2-DOF spherical parallel mechanism.

maintaining a constant relative position and posture. When the relative position and orientation between the mounts change, the end effector rotates around the Y-axis (pitch axis) based on the difference in rotation angle between the mounts.

A unique characteristic of this mechanism is that when operating it in the pitch axis, the direction β in which the mounts push and pull the shaft continuously varies depending on the posture of the end effector. Therefore, the link and joint configuration

and the control method must be considered, which are generally not required when designing a conventional plane type 2-DOF parallel link mechanism.

For example, a revolute pair between the upper and lower arc sliders must be arranged in the mounts as a way to absorb the change in β. Without these rotating joints, the mechanism cannot swing in the pitch axis.

By arranging these revolute pairs, the end effector rotation will not be constrained around the Z-axis (yaw axis). Therefore, an additional link to constrain the rotation in the yaw axis is required. One way to solve this problem is to add a passive mount without a rotational pair between the left and right mounts and attach an arc-shape frame sliding from the passive mount to the end effector. This configuration can uniquely determine the posture of the end effector while the entire device maintains a symmetrical structure.

Furthermore, since the angle β changes depending on the posture, the rotational output in the pitch direction is non-linear and should be considered when operating in the pitch direction.

C. Theoretical Analysis

In this section, the forward and inverse kinematics are solved to determine the relationship between the position of the mount and the posture of the end effector. Accordingly, the characteristics of the non-linear output in the pitch direction described in the previous section are also geometrically analyzed. Additionally, the workspace and singular posture are also analyzed based on kinematics.

1) Forward Displacement Analysis: The roll angle θ_r and pitch angle θ_p of the end effector are initially described using the left and right mount rotation angles φ_1 and φ_2, respectively. The swing direction ψ and the swing displacement angle, which are variables representing the end effector's position of this mechanism, are then described using the roll angle θ_r and the pitch angle θ_p, respectively.

Fig. 4 shows the geometric conditions when an end effector composed of an arc frame with a radius of 1 is rotated in the pitch direction with the origin O as the center of rotation. P_1 and P_2 on the sphere O denote the positions of input mount A and B in Fig. 3, respectively. Q is the point where the end effector frames intersect. R is the midpoint of P_1 and P_2, and S is the point perpendicular to OQ from R.

In ΔSP_1R and ΔOP_1R, the length of P_1R and SR can be expressed in two ways using the rotation angles φ_1 and φ_2 of the left and right mounts and the pitch angle θ_p or the intersecting angle. Therefore, as shown in (1), the relational expression holds.

$$\begin{cases} \left| \overline{P_1R} \right| = SP_1 \sin \frac{\alpha}{2} = OP_1 \sin \frac{\varphi_1-\varphi_2}{2}. \\ \left| \overline{SR} \right| = SP_1 \cos \frac{\alpha}{2} = OP_1 \cos \frac{\varphi_1-\varphi_2}{2} \sin \theta_p. \end{cases} \tag{1}$$

By solving (1) for θ_p, the roll angle θ_r and the pitch angle θ_p can be expressed as shown in (2) using the rotation angles φ_1 and φ_2 of the left and right mounts and the intersecting angle α.

$$\begin{cases} \theta_r = \frac{\varphi_1+\varphi_2}{2}. \\ \theta_p = \sin^{-1}\left(\frac{\tan \frac{\varphi_1-\varphi_2}{2}}{\tan \frac{\alpha}{2}} \right). \end{cases} \tag{2}$$
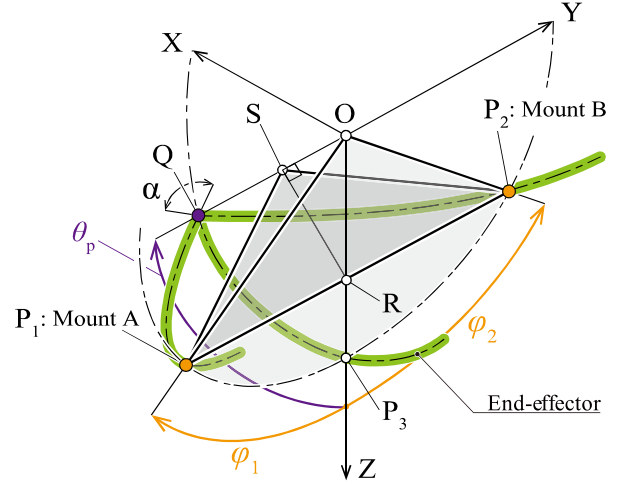

Fig. 4. Geometric conditions when the end effector is rotated in the pitch direction with the origin O as the center of rotation.

The length of the arc P_1P_3 is $(\varphi_1-\varphi_2)/2$ and the length of the arc P_3Q is θ_p. The angle of the spherical angle $P_3Q\,P_1$ is $\alpha/2$. Applying law of Sines of spherical trigonometry to the spherical triangle P_1P_3Q, equation (3) is satisfied that includes the pressure angle β representing spherical angle Q P_1P_3.

$$\frac{\sin \frac{\varphi_1-\varphi_2}{2}}{\sin \frac{\alpha}{2}} = \frac{\sin \theta_p}{\sin \beta}. \tag{3}$$

Therefore, equation (3) can be rewritten using (2), and the pressure angle β can be expressed as follows

$$\beta = \sin^{-1}\left(\frac{\cos \frac{\alpha}{2}}{\cos \frac{\varphi_1-\varphi_2}{2}} \right). \tag{4}$$

Equation (4) shows that pressure angle β is described by φ_1 and φ_2.

Further, the end effector's posture can be described by the X–Y–Z Euler angles, similar to when describing the attitude of the two-joint serial link robot [18]. This is because the end effector in this mechanism rotates $-\theta_r$ around the X-axis and then θ_p around the Y'-axis on the rotated X'Y'Z' axis, as shown in Fig. 5. The posture in this condition can be described as in (5), using θ_r and θ_p.

$$\begin{aligned} {}_{B}^{A}R_{X'Y'Z'} &= R_X(-\theta_r) R_Y(\theta_p) R_Z(0) \\ &= \begin{bmatrix} \cos\theta_p & 0 & \sin\theta_p \\ -\sin\theta_r\sin\theta_p & \cos\theta_r & \sin\theta_r\cos\theta_p \\ -\cos\theta_r\sin\theta_p & -\sin\theta_r & \cos\theta_r\cos\theta_p \end{bmatrix}. \end{aligned} \tag{5}$$

The swing direction ψ and the swing displacement angle θ can be described by θ_r and θ_p as follows.

$$\begin{cases} \psi = \tan^{-1}\frac{\tan\theta_p}{\sin\theta_r}. \\ \theta = \cos^{-1}\left(\cos\theta_r \cos\theta_p \right). \end{cases} \tag{6}$$

By differentiating (2) and (6), the velocity of the end effector can be obtained.

2) Inverse Displacement Analysis: Subsequently, equations (7) and (8) can be derived by back calculation of (2) and (6) of
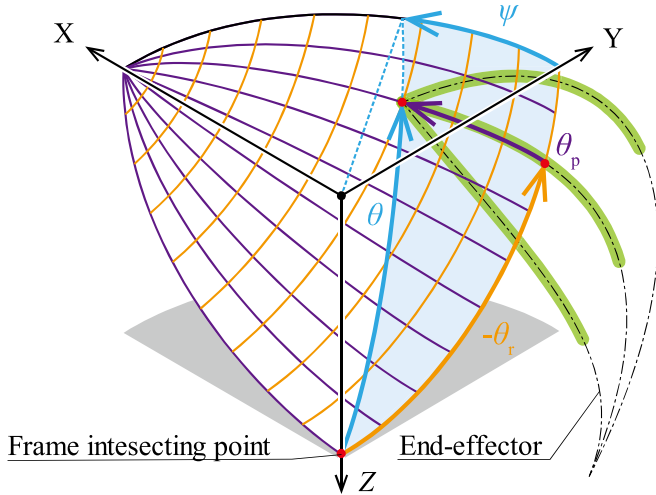
Fig. 5. Displacement analysis.

Fig. 6. Passive prototype model overview.

forward kinematics.

$$\begin{cases} \varphi_1 = \theta_{\mathrm{r}} + \tan^{-1}\left(\tan\frac{\alpha}{2}\sin\theta_{\mathrm{p}}\right). \\ \varphi_2 = \theta_{\mathrm{r}} - \tan^{-1}\left(\tan\frac{\alpha}{2}\sin\theta_{\mathrm{p}}\right). \end{cases} \quad (7)$$

$$\begin{cases} \theta_{\mathrm{r}} = \tan^{-1}\left(\cos\psi\tan\theta\right). \\ \theta_{\mathrm{p}} = \sin^{-1}\left(\sin\theta\sin\psi\right). \end{cases} \quad (8)$$

3) Workspace / Singular Posture: This mechanism can rotate 360° infinitely in the roll direction without any singular posture and has a wide working area. This is a unique feature not observed in conventional 2-DOF SPMs.

Conversely, the movable range in the pitch direction is 180°, and when $\theta_{\mathrm{p}} = 90°$, the end effector transfers to a singular posture. Therefore, when a work area exceeding 90° is required, a mechanism to avoid the singular posture is also required. Interference between parts occurs when the pitch angle is near 0°. Design sliders to avoid interference may secure a large work area.

III. MECHANICAL DESIGN

In order to demonstrate that the movement of the prototype can be obtained based on the principles, a manual passive-type model was fabricated. The electric active prototype model was designed to demonstrate a method using an arc rack gear as the driving method of the slider while verifying its characteristics in the prototype.

A. Passive Model

Fig. 6 shows a passive prototype model. The mechanical design was made assuming that the left and right sliders would be operated manually. The prototype comprised a base frame, driving sliders A and B, a passive slider C, and an end effector link. The base frame and end effector were constructed from a 3D printed acrylic resin, and the slider rollers were milled from an aluminum plate. The acrylic base frame is fixed to the aluminum base and acts as an arc-shaped rail. Three sliders passively rotate along with it when operating them manually.
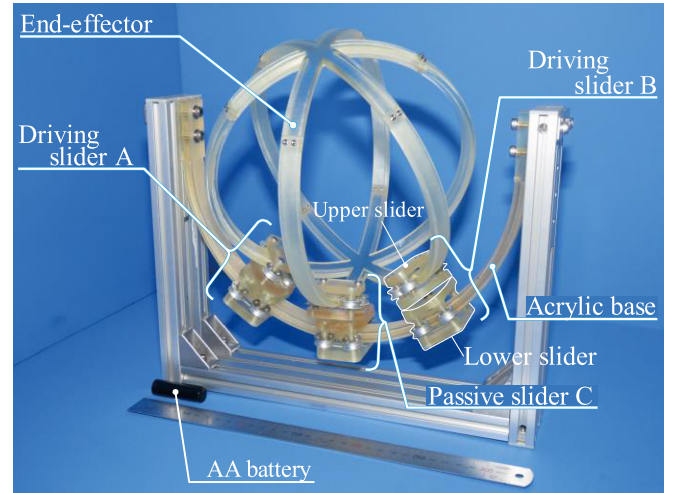
TABLE II
ACTIVE PROTOTYPE MODEL PROPERTIES

Height	355	mm
Width	385	mm
Depth	370	mm
Weight (whole)	9212	g
Weight (only end effector)	273	g
Radius of end effector	102	mm
Intersecting angle α	120	deg

The driving sliders A and B act as left and right mounts shown in Fig. 3. The sliders A and B are connected to the acrylic base frame via rollers at the lower slider. The upper slider acts as a slider for each axis of the end effector frame. Bearings are installed between the upper and lower sliders, and thus sliders A and B rotate freely by themselves.

The passive slider C is a mount located in the middle of the driving sliders. The role of the upper and lower sliders is the same as that of the sliders A and B. Unlike the sliders A and B, the upper and lower sliders of the slider C comprise a single piece, and they are designed to ensure their direction is consistently orthogonal.

The end effector was constructed by crossing three arc-shaped frames. The intersecting angle α of the left and right shaft axes was set to 120°, and the central frame axes intersected at an angle bisected. By extending the arc-shaped frames and making the end effector a sphere, the center of mass of the end effector and the center of rotation meet at one point so that the end effector does not rotate due to the influence of gravity.

B. Active Model

Fig. 1 shows an active prototype model with the left and right electrified sliders. Table II shows the properties of the active prototype. Fig. 7 shows a three-view of the active prototype model, which consisted of two 20-W geared motors with a 139:1 gear ratio, active sliders with arc rack gears, a passive slider C, an end effector link, and a base. The end effector link and arc
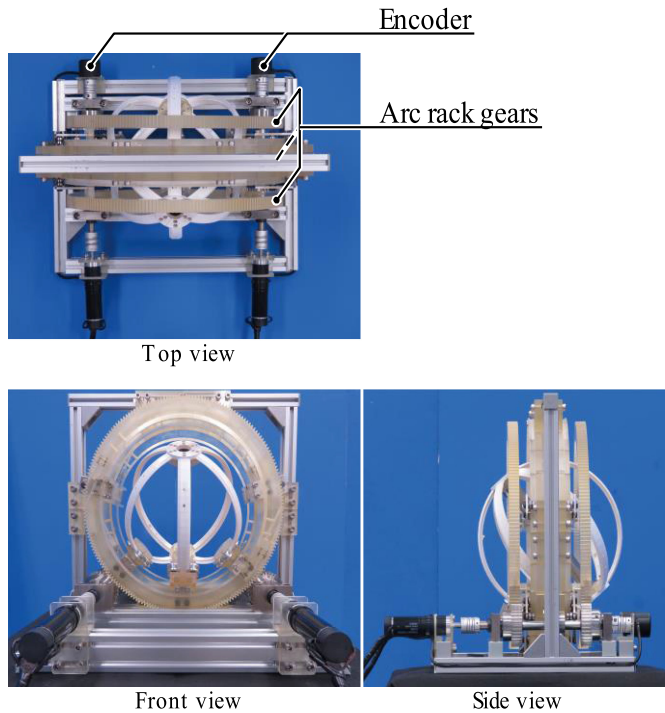
Fig. 7. Three views of active prototype model.

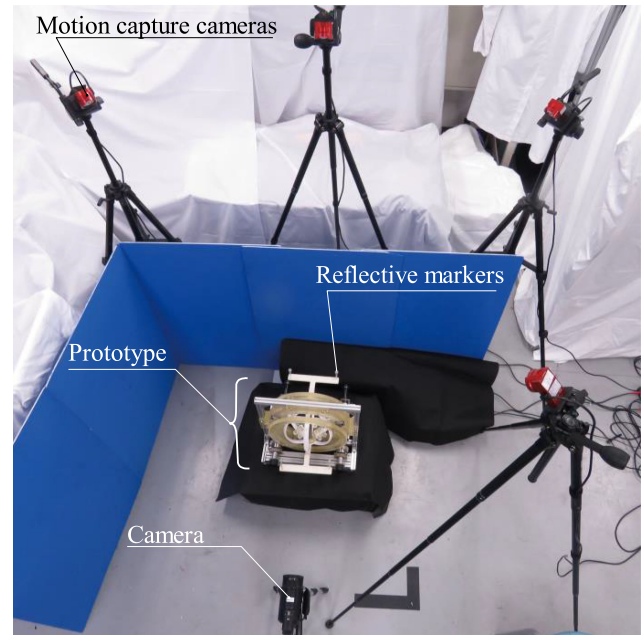Fig. 8. Overview of the experiment setup, which consists of four motion capture cameras, the prototype with reflective markers, and a video camera.

rack gears were built using 3D printed acrylic resin, and the slider roller was made of milled aluminum.

The motor transmits the driving force to the arc rack gear via the shaft and spur gear. The A and B sliders with arc rack gears shown in Fig. 1 are connected to the arc rails of the base parts via rollers. Three arc rack gears are arranged in parallel in the depth direction.

When the central rack gear receives the torque from motor A, slider A rotates with the rack gear. When the rack gears on both ends are actuated from motor B, slider B rotates with both gears.

Similar to the passive model, the upper and lower sliders are connected via bearings allowing sliders A and B to rotate freely by themselves. Similar to sliders A and B, the passive slider C slides along the arc-shaped rail of the base part via rollers. Slider C moves passively between sliders A and B in response to the movement of the end effector. The upper and lower sliders comprise a single piece, thus ensuring the direction of the bottom and upper sliders is consistently orthogonal.

The end effector has the same shape as that in the passive model. One shaft was installed in the center to reduce frame bending.

The range of motion without interference is $-\infty \leq \theta_r \leq \infty$ and $15° \leq \theta_p \leq 90°$ in the prototype.

Here, in order to estimate the range in which the accurate pitch rotation output can be obtained, the friction-reducing characteristics of the rollers with the end effector must be considered in prototype manufacturing.

Generally, the movement of rollers degrades due to the influence of frictional resistance when the pressure angle β is about 60° or more. Using (2) and (4), the limit of the pitch rotation angle $\theta_p = 54°$ when $\beta = 60°$.

IV. BASIC EXPERIMENT AND RESULTS

We measured the roll angle θ_r and pitch angle θ_p of the active type model to evaluate the workspace of this mechanism and confirm whether the target angle can be achieved. As shown in Fig. 8, the posture changes were recorded by four motion capture cameras when the end effector was rotated in the roll and pitch directions. The left and right mount rotation angles, φ_1 and φ_2 respectively, were calculated from the rotation angles of the encoders mounted on the backside of the motor shafts.

A. Roll Motion Measurement

The end effector was rotated in the roll direction while keeping $\theta_p = 42°$. Fig. 9(1–6) shows a series of snapshots taken from the video of the back of the prototype. After setting the initial position to $\varphi_1 + \varphi_2 = 0°$, the motor was rotated until $\varphi_1 + \varphi_2$ became -180°, and then the motor was reversed until $\varphi_1 + \varphi_2$ became 180°. This operation was performed three times. As a typical example of the experimental results, Fig. 10 shows the relationship between the positions φ_1 and φ_2 of the A and B sliders and the roll angle θ_r of the end effector in one trial.

As a result of the three trials, the measured values for θ_r had an average error of 2.5° and a maximum error of 7.7° when compared to the theoretical values. Initially, the error tended to increase as $\varphi_1 + \varphi_2$ decreased, but an error larger than average tended to occur in the range around $\varphi_1 + \varphi_2 = -180°$. On average, this range lasts from $\varphi_1 + \varphi_2 = -137.8°$ to 45.7°. The error tended to decrease after $\varphi_1 + \varphi_2$ reached 0°.

B. Pitch Motion Measurement

The end effector was rotated in the pitch direction while keeping $\theta_r = 0°$. Fig. 11(1–6) shows a series of snapshots taken
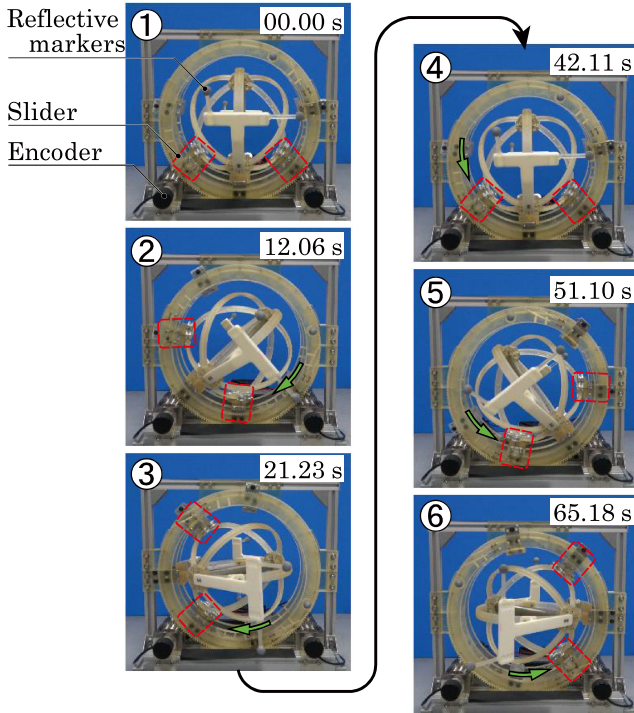
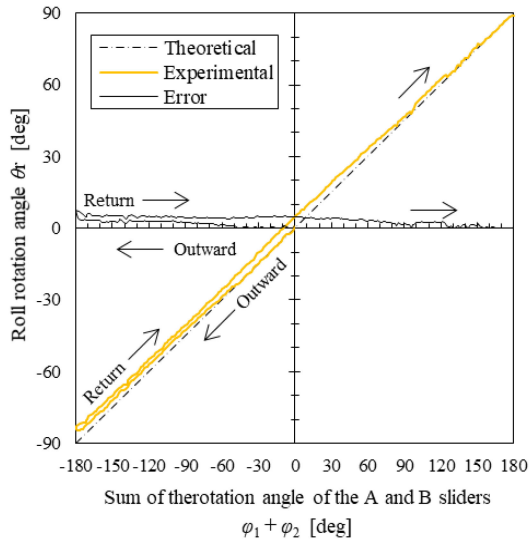Fig. 9.   Series of snapshots taken of the prototype (roll motion).

Fig. 10.   End effector roll rotation angle.

Fig. 11.   Series of snapshots taken of the prototype (pitch motion).

Fig. 12.   End effector pitch rotation angle.

from the video of the back of the prototype. After setting φ_1-φ_2 = 46° as the initial state, the end effector was rotated forward until φ_1-φ_2 = 110° and then reversed until φ_1-φ_2 = 46°. This operation was performed five times. The initial state is when φ_1-φ_2 is the lowest and without interference between the sliders.

Fig. 12 shows the typical relationship between positions φ_1 and φ_2 of the A and B sliders and the pitch angle θ_{p} of the end effector in one trial. As a result of the five trials, the measured values for θ_{p} had an average error of 1.0° and a maximum error of 8.1° compared to the theoretical values. The trajectory of the graph varied between the outward and the return routes, and
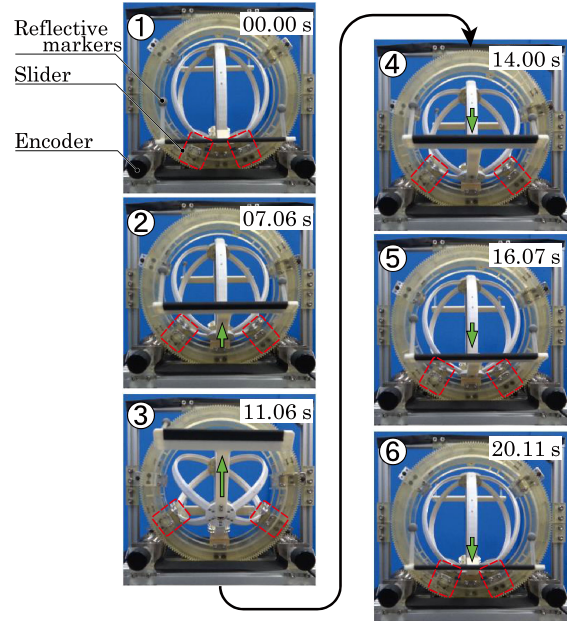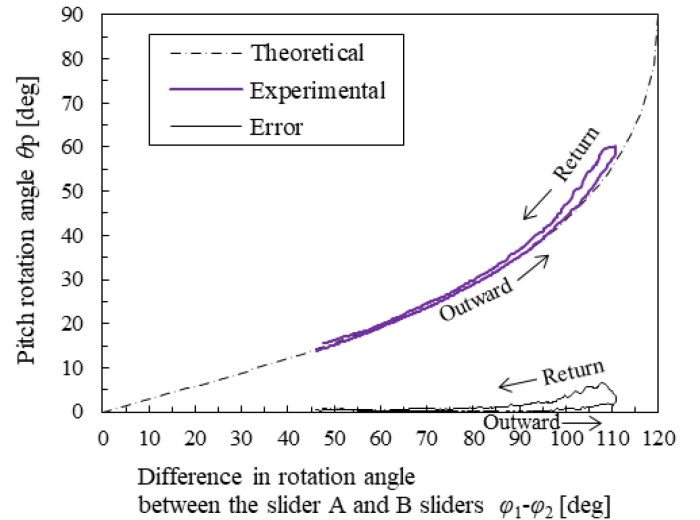
hysteresis was confirmed. The error of the return route tended to be larger than that of the outward route. Before and after φ_1-φ_2 = 110°, there was a tendency for an error larger than average to occur. On average, this range was from φ_1-φ_2 = 100.6° to 92.6°.

V. DISCUSSION

The primary cause of error in the roll angle θ_{r} is the influence of gravity on the end effector. When the end effector height increases, the error increases in the range where $\varphi_1 + \varphi_2$ decreases from 0° to -180° or increases from 0° to 180°, as shown in Fig. 10.

This misregistration is likely to occur when the wobble of the mount components increases. Therefore, in this prototype, reducing the error by increasing the shaft diameter used in the
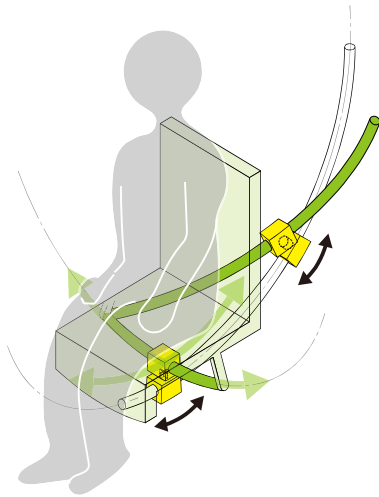
Fig. 13. Image of applying curved biaxial mechanism to a sheet.

upper and bottom sliders in the mount and the roller support shaft is considered effective.

Conversely, the main factor that causes the error of the pitch angle θ_p is the end effector shaft deflection. Fig. 12 shows that the error increases when φ_1-φ_2 is large. In this range, the angle of β and the normal force applied to the shaft are both large, thus a large shaft deflection occurs.

To reduce the end effector deflection, constructing the frame shaft of the end effector from a more rigid material such as metal is considered effective.

VI. CONCLUSION

We proposed an 8R slider type 2-DOF SPM, also known as a curved biaxial swing mechanism, with multiple arc sliders and a Λ-shaped end-effector. This mechanism can control the posture of the Λ-shaped end effector so that two frames can intersect at a fixed angle by controlling the positions of the two arc sliders.

In this study, we solved the forward and inverse kinematics for posture control of the end effector, constructed a design method, and manufactured a prototype. We also measured and clarified the basic driving characteristics of the prototype.

As a result of the experiment, the average roll angle error compared to the theoretical value was 2.5°, and the average pitch angle error was 1.0°. In future studies, we aim to increase the size of the support parts to reduce wobbling and the posture error of the end effector. We also plan to increase the rigidity by constructing the end effector from metal.

We believe a new closed-loop control system would reduce errors throughout the system. The current configuration uses only the rotation angle of the motor obtained from the encoder for input. However, a new end effector IMU could sense both the direction and angular velocity for feedback to the input [12] [13].

Furthermore, we will experiment to clarify the transmission efficiency of the mechanism and establish a control method based on inverse kinematics.

We also plan to install the proposed mechanism in automobiles and apply it to the stabilization platform and the acceleration reduction mechanism [3], as shown in Fig. 13.

REFERENCES

[1] K. Maeda, S. Tadokoro, T. Takamori, M. Hiller, and R. Verhoeven, "On design of a redundant wire-driven parallel robot WARP manipulator," in *Proc. 1999 IEEE Int. Conf. Robot. Automat.*, 1999, vol. 2, pp. 895–900.

[2] Y. Takeda, "Parallel mechanism," *J. Jpn. Soc. Precis. Eng.*, vol. 71, no. 11. pp. 1363–1368, 2005.

[3] M. Nobutoki and S. Suzuki, "Development of a tilting system for reducing horizontal acceleration in cars," in *Proc. Soc. Automot. Engineers Jpn. Autumn Meet.*, 2019.

[4] C. M. Gosselin and F. Caron, "Two degree-of-freedom spherical orienting device," US Patent 5966991, Oct. 19, 1999.

[5] W. Cao, S. Xu, K. Rao, and T. Ding, "Kinematic design of a novel two Degree-of-Freedom parallel mechanism for minimally invasive surgery," *J. Mech. Des.*, vol. 141, no. 10, pp. 1–7 2019.

[6] X. Kong, "Forward displacement analysis of a 2-DOF RR-R_RR-RRR spherical parallel manipulator," in *Proc. IEEE/ASME Int. Conf. Mechatronic Embedded Syst. Appl.*, 2010, pp. 446–451.

[7] G. R. Dunlop and T. P. Jones, "Position analysis of a two DOF parallel mechanism—The Canterbury tracker," *Mechanism Mach. Theory*, vol. 34, no. 4, pp. 599–614, 1999.

[8] M. Jiang, X. Hu, L. Liu, and Y. Yu, "Study on Parallel 2-DOF Rotation Mechanism in Radar," *Phys. Procedia*, vol. 24, pp. 1830–1835, 2012.

[9] S. Kulkarni, S. Tonapi, P. Larochelle, and K. Mitra, "Effect of tracking flat reflector using novel auxiliary drive mechanism on the performance of stationary photovoltaic module," in *Proc. ASME Int. Mech. Eng. Congr. Expo.*, WA, USA, 2007, vol. 6, pp. 351–356.

[10] A. Cammarata, "Optimized design of a large-workspace 2-DOF parallel robot for solar tracking systems," *Mechanism Mach. Theory*, vol. 83, pp. 175–186, 2015.

[11] R. Baumann, W. Maeder, D. Glauser, and R. Clavel, "The PantoScope: A spherical remote-center-of-motion parallel manipulator for force reflection," in *Proc. Int. Conf. Robot. Automat.*, 1997, vol. 1, pp. 718–723.

[12] S. Ansari-Rad, M. Zarei, M. G. Tamizi, S. Mohammadi Nejati, M. T. Masouleh, and A. Kalhor, "Stabilization of a Two-DOF Spherical Parallel Robot via a Novel Adaptive Approach," in *Proc. 6th RSI Int. Conf. Robot. Mechatronics (IcRoM)*, 2018, pp. 369–374.

[13] B. Danaei, M. Alipour, A. Arian, M. T. Masouleh, and A. Kalhor, "Control of a two degree-of-freedom parallel robot as a stabilization platform," in *Proc. 5th RSI Int. Conf. Robot. Mechatronics (ICRoM)*, 2017, pp. 232–238.

[14] M. E. Hesar, M. T. Masouleh, A. Kalhor, M. B. Menhaj, and N. Kashi, "Ball tracking with a 2-DOF spherical parallel robot based on visual servoing controllers," in *Proc. 2nd RSI/ISM Int. Conf. Robot. Mechatronics (ICRoM)*, 2014, pp. 292–297.

[15] E. Samson, D. Laurendeau, M. Parizeau, S. Comtois, J. F. Allan, and C. Gosselin, "The agile stereo pair for active vision," *Mach. Vis. Appl.*, vol. 17, no. 1, pp. 32–50, 2006.

[16] M. Carricato and V. Parenti-Castelli, "A novel fully decoupled two-degrees-of-freedom parallel wrist," *Int. J. Robot. Res.*, vol. 23, no. 6, pp. 661–667, 2004.

[17] J. J. Cervantes-Sánchez, J. C. Hernández-Rodríguez, and E. J. González-Galván, "On the 5R spherical, symmetric manipulator: Workspace and singularity characterization," *Mechanism Mach. Theory*, vol. 39, no. 4, pp. 409–429, 2004.

[18] L. J. Zhang, Y.-W. Niu, Y.-Q. Li, and Z. Huang, "Analysis of the workspace of spherical 2-DOF spherical 5R parallel manipulator," in *Proc. IEEE Int. Conf. Robot. Automat.*, 2006, pp. 1123–1128.

[19] B. Danaei, A. Arian, M. Tale masouleh, and A. Kalhor, "Dynamic modeling and base inertial parameters determination of a 2-DOF spherical parallel mechanism," *Multibody System Dyn.*, vol. 41, pp. 367–390, 2017.

[20] X. Kong, "Forward Displacement Analysis and Singularity Analysis of a Special 2-DOF 5R Spherical Parallel Manipulator," *J. Mechanisms Robot.*, vol. 3, no. 2, 2011.

[21] A. Horie, A. Nomura, K. Tadakuma, M. Konyo, H. Nagano, and S. Tadokoro, "Enhancing Haptic Experience in a Seat with Two-DoF Buttock Skin Stretch," *Asia Haptics 2018*, 2019, pp. 134–138.

[22] J. Craig, "Spatial Transformations," in *Robotics—Mechanism/Kinematics/Control—*, M. Nanjyo, Ed., 1st ed., Tokyo, Japan: Kyoritsu Shuppan (in Japanese), 1991, ch. 2, sec. 8, pp. 45–46.